Journal of Hazardous Materials Letters 5 (2024) 100134

Contents lists available at ScienceDirect

Journal of Hazardous Materials Letters

journal homepage: www.sciencedirect.com/journal/journal-of-hazardous-materials-letters

μ-X-ray fluorescence (XRF) and fluorine K-edge μ-X-ray absorption near-edge structure (XANES) spectroscopy for detection of PFAS distribution in the impacted concrete

Phong H.N. Vo [a,b,1], Christian Vogel [c,1,*], Hong T.M. Nguyen [a,d], Brett R. Hamilton [e], Phong K. Thai [a], Philipp Roesch [c], Franz-Georg Simon [c], Jochen F. Mueller [a]

[a] Queensland Alliance for Environmental Health Sciences (QAEHS), The University of Queensland, QLD 4102, Australia
[b] Climate Change Cluster, Faculty of Science, University of Technology Sydney, 15 Broadway, Ultimo, NSW 2007, Australia
[c] Bundesanstalt für Materialforschung und -prüfung (BAM), Division 4.3 – Contaminant Transfer and Environmental Technologies, Unter den Eichen 87, Berlin 12205, Germany
[d] Ramboll Australia Pty Ltd, 100 Pacific Highway, North Sydney, NSW 2060, Australia
[e] Centre for Microscopy and Microanalysis, The University of Queensland, St. Lucia, QLD 4072, Australia

ARTICLE INFO

Keywords:
AFFFs
PFAS
Concrete
Fluorine K-edge μ-XANES spectroscopy
μ-XRF

ABSTRACT

An improved understanding of the distribution of per- and polyfluoroalkyl substances (PFAS) in PFAS-impacted concrete is important for risk management and decontamination of PFAS. This study incorporates μ-X-ray fluorescence (μ-XRF) and fluorine K-edge μ-X-ray absorption near-edge structure (μ-XANES) spectroscopy to gain non-destructive insights into PFAS distribution in the impacted concrete. The μ-XRF and μ-XANES spectroscopy provided additional details on the detection of PFAS, which were not detected by the desorption electrospray ionization (DESI) imaging method conducted previously. The shorter chain PFAS were found on the top part of the concrete core (0.5 cm), and longer chain PFAS were mostly at the bottom part of the concrete core (5 cm). The inorganic fluorine fraction was also detected, and it likely hampered the detection of organic fluorine such as PFAS in the concrete. Thus, this non-destructive technique is an complementary approach to detect PFAS in contaminated concrete.

1. Introduction

Per- and polyfluoroalkyl substances (PFAS) are the active ingredient of aqueous film-forming foams (AFFFs) that have been used widely for firefighting training purposes. That practice has led to PFAS contamination in the concrete slabs at firefighting training grounds (FTGs) (Douglas et al., 2023). Concrete structures in FTGs have often accumulated PFAS over time and now act as an ongoing source of releasing PFAS to the surrounding environment (Baduel et al., 2015). Restricting the use of PFAS-containing AFFFs is therefore increasingly important to prevent leaching of PFAS when decontaminating FTGs.

The efficacy of PFAS decontamination or leaching prevention depends on the precise characterization of PFAS distribution across the whole surface and depth of an impacted FTG. However, studies on the depth distribution of PFAS-impacted FTGs are still limited. There have been two main approaches developed for that purpose, including drilling samples along the depth of a concrete core collected from impacted FTGs (Baduel et al., 2015; Thai et al., 2022). The samples are then extracted by solvent and subjected to PFAS quantification by liquid chromatography-tandem mass spectrometry (LC-MS/MS). Recently, Vo et al. (2023) used mass spectrometry imaging in the form of desorption electrospray ionization (DESI) to visualize the distribution of PFAS. The LC-MS/MS technique is a quantitative method for a wide range of PFAS compounds. Meanwhile, it is a time-consuming process from sample preparation to quantification, and the lack of capacity to understand the distribution of PFAS across the concrete in high-resolution details. DESI imaging has demonstrated its advantages in the high-resolution distribution of PFAS at 30–200 μm pixel size; however, it has been limited to PFHxS (C_6) and PFOS (C_8), and its sensitivity needs improvement to capture the lower-occurrence PFAS (Vo et al., 2023).

* Corresponding author.
E-mail address: christian.vogel@bam.de (C. Vogel).
[1] Phong H. N. Vo and Christian Vogel contributed equally to this paper.

https://doi.org/10.1016/j.hazl.2024.100134
Received 8 July 2024; Received in revised form 5 November 2024; Accepted 10 November 2024
Available online 14 November 2024

An integrative method, which infuses μ-X-ray fluorescence (μ-XRF) mapping and μ-X-ray absorption near-edge structure (μ-XANES) spectroscopy has been developed to characterize chemical (e.g., phosphorus, heavy metals, PFAS) spatially in consumer products (e.g., textiles, food packaging materials) and environmental samples (e.g., soils, sludges) with promising results (Roesch et al., 2023; van der Bom et al., 2022; Vogel et al., 2016). μ-XRF mapping is applicable for the high-resolution detection of element hotspots in samples, coupling with μ-XANES spectroscopy as an advanced method to identify the chemical bonding of an element. Organofluorinated compounds exhibit characteristic XANES spectral patterns at the fluorine K-edge depending on chain length (ultrashort, short, and long) and fluorine content (perfluorinated, partially fluorinated), and thus can be distinguished from inorganic fluorine compounds (Roesch et al. 2022, Roesch et al. 2023). The penetration depth of the analytical beam produced by μ-XRF/μ-XANES spectroscopy is approximately 1 μm at the fluorine edge energy which is much deeper than X-ray photoelectron spectroscopy (XPS; only approx. 10 nm). It enables the μ-XANES spectroscopy to detect chemicals of interest in the near-surface region. The application of those two detection techniques improves the sensitivity and reliability of chemical detection. The PFAS-impacted concrete is considered a new matrix that would be worthy of applying μ-XRF mapping and fluorine K-edge μ-XANES spectroscopy for identification of PFAS distribution.

This study aims to assess the incorporation of μ-XRF mapping and μ-XANES spectroscopy as a new non-destructive tool for PFAS-impacted concrete. This study focuses on investigating the capabilities and limitations of this technique in characterizing PFAS within concrete.

2. Materials and methods

2.1. Concrete samples

The impacted concrete used in this study has been described previously (Thai et al., 2022; Vo et al., 2023). In brief, the concrete core (code D_2) was extracted from an impacted FTG in Australia. This core and its vertical slices were previously analyzed using DESI and core sidewall drilling methods, now being used for μ-XRF incorporated μ-XANES (Thai et al., 2022; Vo et al., 2023). Samples were prepared by sectioning the core using a dry cut. The concrete slice after sectioning was subject to another cut to fit into the sample holder for both DESI and μ-XRF incorporated μ-XANES methods (Fig. 1). The size of the concrete sample for μ-XRF incorporated μ-XANES method is 5 cm×2 cm x 1 cm (depth x width x thickness). In addition, a reference blank concrete sample, collected at The University of Queensland (Australia), was used as background. This blank sample is free of PFAS, which has been shown previously (Vo et al., 2023).

2.2. Chemical standards for μ-XRF and fluorine K-edge μ-XANES

The following PFAS standards were used for XANES calibration: sodium trifluoromethyl sulfonate (TFMS, 98 %, BLD pharma), potassium perfluorobutyl sulfonate (PFBS, 98 %, Sigma Aldrich), potassium perfluorohexyl sulfonate (PFHxS, ≥ 98 %, Sigma Aldrich), perfluorooctanesulfonic acid (PFOS, 97 %, ABCR), perfluorooctanecarboxylic acid (PFOA, 96 %, SigmaAldrich) and 1 H,1 H,2 H,2H-perfluorooctanesulphonic acid (6:2-FTS, 97 %, abcr).

2.3. Sample preparation and detection by fluorine μ-XANES spectroscopy

All solid reference compounds were prepared as a thin layer of a few milligrams spread on a fluorine-free carbon tape. The concrete sample was taped directly to the copper sample plate. On the concrete sample, three μ-XRF line scans with a lateral resolution of 100 μm from top to bottom were performed (Fig. 1). Afterwards, in areas where fluorine hotspots could be found, eight fluorine K-edge μ-XANES measurements per line scan were performed.

2.4. μ-XRF and μ-XANES spectroscopy

The μ-XRF lines and fluorine K-edge μ-XANES spectra were collected

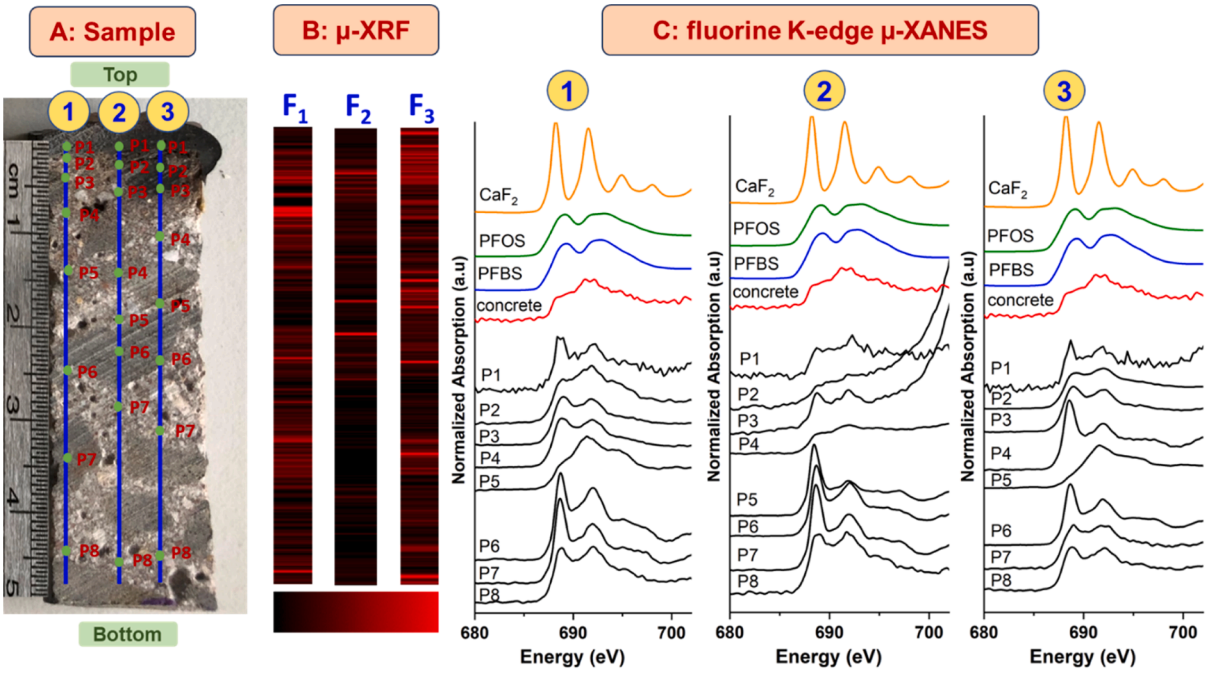

Fig. 1. (A) Concrete sample with three line scans (1,2,3) and green marked spots where the samples got beamed for μ-XANES (P_1-P_8); (B) μ-XRF fluorine line scans (F_1, F_2, F_3). Images were produced using a color gradient (black to red) where the largest intensity is indicated by an intense red and (C) fluorine K-edge μ-XANES spectra of references, and the beamed spots from the three-line scans. The scan resolution is 100 μm and the color scale is arbitrary. All μ-XRF maps span 100 μm spot size. Each μ-XANES spectra is organized to avoid the overlapping of the peak at 688.7–691.7 eV. The strong increase at high energy of some XANES spectra is due to interference of the iron L-edge.

on the PHOENIX II beamline of the Swiss Light Source (SLS, Villigen, Switzerland). The μ-XRF spectra were batch-fitted at each map pixel using the PyMca software (Solé et al., 2007). The μ-XANES spectra were normalized and background corrected using the Athena software from the Demeter 0.9.26 package (Ravel and Newville, 2005). More information's and examples for the linear combination (LC) fitting procedure of the data (Fig. S1 and Fig. S2) are shown in the supporting information.

3. Results and discussion

3.1. Fluorine K-edge μ-XANES spectroscopy of PFAS standards

The spectra of PFAS standards captured by XANES analysis are shown in Fig. S3. All six studied PFAS show similar characteristics (least pronounced with TFMS) in which two peaks are featured at 688.7 eV and 691.7 eV, then followed by only very weak features in the post-edge region after 700 eV. The results are in agreement with the two previous studies that analyzed bulk XANES and STXM-XANES for PFAS (Roesch et al., 2022; Yan et al., 2021). Each PFAS compound is differentiated by the relative ratio of peak intensity at 688.7 eV and 691.7 eV. The peak at 688.7 is attributable to the F 1 s → σ* C-F transition of the C-F bond (Yan et al., 2021). The shorter chain PFAS species are associated with higher peak intensity at 691.7 eV, hence their ratio is higher than the longer chain PFAS (Roesch et al., 2022). In principle, the absolute quantification of the ratio can be used to infer the chain length relevant PFAS in the matrix (Table 1 and Table S1). However, it must be kept in mind that the presence of inorganic fluoride can hamper the analysis, and hence, a more complex analysis, for example by linear combination fitting is required.

The unique characteristic of the PFAS spectrum is distinct from the inorganic fluoride chemicals, which have a wide range of spectrum shapes (see Fig. S4). For example, the spectrum of CaF_2 exhibits a sharp white line at 688.0 eV and further sharp features at 691.3, 694.7, 697.8, and 702.6 eV. Fluorapatite has a similar white line at 687.8 eV but only two additional spectral features at 691.1 and 696.2 eV. Moreover, FeF_3 has a large pre-peak at 683.3 eV and a broad white line between 689.0 and 693.0 eV. In addition, spectra of AlF_3 and Na_2SiF_6 have only a few features – AlF_3 has two major peaks at 692 eV and 697.5 eV, and Na_2SiF_6 has a broad white line between 685 and 700 eV (Roesch et al. 2022, Roesch et al. 2023). The difference can be attributed to the response of C-F bonding to the amorphous PFAS molecule. Whilst due to the crystallinity, the bonding of inorganic fluoride (e.g., Na-F, Al-F, K-F) responds to more features in different energy (Roesch et al. 2023).

Table 1
The ratio of the normalized intensity of the features at 688.7 eV and 691.7 eV in PFAS standards and selected concrete samples (ratios of all concrete samples are in Table S1).

	Blank	TFMS (C_1)	PFBS (C_4)	PFHxS/6:2 FTS (C_6)	PFOS (C_8)	PFOA (C_7)
Standards	0.606	0.784	0.918	0.967	0.984	1.087
Line scan 1 – P_2	-	0.724 *	-	-	-	
Line scan 1 – P_8	-	-	-	-	0.988 *	-
Line scan 2 – P_3	-	-	0.929 *	-	-	-
Line scan 2 – P_8	-	-	0.934 *	-	-	-
Line scan 3 – P_2	-	-	0.881 *	-	-	-
Line scan 3 – P_7	-	-	-	0.957	-	-
Line scan 3 – P_8	-	-	-	-	-	1.081

* The asterisk indicates the imperfect matches with the standard

3.2. μ-XRF mapping and Fluorine K-edge μ-XANES spectroscopy of the impacted sample

The fluorine μ-XRF line scans and μ-XANES spectroscopy of the impacted concrete sample are shown in Fig. 1. Fluorine μ-XRF line scans display in red the fluorine hotpots. Fig. S5 – S7 show additionally combined fluorine, carbon, and oxygen maps of the three-line scans with the minimum and maximum number of counts for each element. While oxygen is almost equally distributed, the asphalt layer on top contains a large amount of carbon and the rest of the concrete sample is almost carbon-free. The overall fluorine amount appears at high intensities at some hotspots: point 2, point 3, point 4, point 7, and point 8 of line scan 1; point 2, point 6 of line scane 2; and point 2, point 3, point 5, point 6, point 7, and point 8 of line scan 3. The results also show that there is an insignificant level of fluorine amount at the top of the core, represented by the black color (number of counts in Fig. S5 – S7) of the μ-XRF mapping and the noisy spectra at P_1 of all three-line scans in fluorine K-edge μ-XANES spectroscopy. The composition of fluorine in the hotspots can be further elucidated by fluorine K-edge μ-XANES.

In line scan 1, the spectra of P_2 and P_5 indicate the presence of shorter chain because TFMS is the major compound in the LC fit (see Table S2). Furthermore, line scan 1, P_2 spectra the 688.7 eV/691.7 eV ratio is 0.724 which is close to that ratio of TFMS (see Table 1). Approaching the bottom of the concrete sample, there is a mix of organic and inorganic fluorine detected. P_3 and P_4 of line scan 1 appear to be other hotspots of organic fluorine (Roesch et al., 2022). The LC fits indicate 6:2-FTS (C_6) and PFOS (C_8) as major PFAS. P_6 and P_7 of line scan 1 are probably unknown inorganic fluorine indicated by sharp peaks at 688.7 eV. Furthermore, the ratio of spot P_8 is between PFOS (C_8) and PFOA (C_7). The LC fit indicate PFAO as major compound in the fit.

Spots P_1, P_2, and P_4 to P_7 of line scan 2 reveal inorganic fluorine. Moreover, no or LCF fits with a high R-value were determined which indicate also unknown inorganic fluorine compounds. However, line scan 2, P_3 and P_8 show the occurrence of PFBS with a 688.7 eV/691.7 eV ratio of 0.929 and 0.934 (close to 0.918 of PFBS standard, Table 1). Furthermore, the LC fits for spots P_6-P_8 indicate the long-chain PFAS 6:2-FTS (C_6) and PFOA (C_7).

For line scan 3, visually there is no PFAS detected at some spots (P_1, and P_4 to P_6), hence the strong signal of μ-XRF scan (P_1 – P_7) in line scan 3 was mainly from inorganic fluoride, which was also confirmed by the LCF of P_5 (see SI). However, P_2 (ratio 0.881) is likely relevant to a shorter chain PFAS such as PFPrS (C_3) which has a 688.7 eV/691.7 eV ratio between 0.784 (TFMS (C_1)) and 0.918 (PFBS (C_4)). At the bottom region P_7 (PFHxS) and P_8 (PFOA), longer PFAS were detected on the 688.7 eV/691.7 eV ratio (Table 1). The presence of long-chain PFAS (PFOS and PFOA) was also determined by the LC fits. The presence of PFOA (C_7) is reasonable because it is a PFAS that might occur on AFFF contaminated concrete (Leeson et al., 2021)

Overall, the occurrence of shorter chain PFAS was confirmed on the top part of the concrete sample (P1, P_2), and the long chain PFAS were detected at the bottom part (P_7 – P_8), especially for line 1 and line 3. There is also a possibility of 6:2 FTS (C_6) and PFOA (C_7) occurring across the concrete core (P_1 – P_8) (1 – 5 cm) which address the gap of the previous studies (Table S2). In the previous ones, the long-chain PFAS (e.g., PFOS (C_8) and PFHxS (C_6)) were detected at the same depth by LC/MS-MS and DESI which agreed with this finding. For example, DESI also detected PFOS (C_8) and PFHxS (C_6) at green-blue color scales which were 0.003 – 0.025 ng/mm^2 for PFHxS (C_6) and 0.004 – 0.038 ng/mm^2 for PFOS (C_8) (Vo et al., 2023). There is a possibility that shorter chain PFAS also occurred at the bottom part of the samples (5 cm), however, more line scans need to be conducted.

The detection limit of this technique has been approximated previously by using quartz sand as a proxy to develop a semi-quantitative method. After spiking a range of PFOS concentrations into quartz sand, the examination showed that 10 μg PFOS/g quartz sand is close to

the detection limit for the bulk-XANES technique (Roesch et al., 2022). However, for the μ-XANES approach, the detection limit could be lowered to 0.1 μg PFOS/g concrete averaged over the whole sample (Roesch et al. 2023). μ-XANES, as an imaging technique can achieve micrometer spatial resolution and therefore can detect PFAS in small regions with relatively high F concentration, which would remain undetected when using averaged signals. The detection limit for PFAS in concrete is preferentially given as PFAS mass per unit of surface area, but it is challenging to reliably obtain it at this stage. Alternatively, the detection limit could be determined by analysis of the powdered or milling concrete to a powder which could be a subject for future improvement of the method.

It is noted that there is still much debate on whether μ-XRF mapping and μ-XANES spectroscopy can be affected by radiation damage, as the photon density in the micro-focussed photon beam can be significantly higher compared to an unfocussed beam. Here we use a modest spot size of 100 μm to check for radiation damage, we also performed a second scan for every μ-XANES spot and detected no significant radiation damage (Fig. 2).

Other techniques such as combustion ion chromatography (CIC) and ^{19}F-nuclear magnetic resonance (NMR) have been used to characterize PFAS in the environmental samples (Camdzic et al., 2021; Shelor et al., 2024). However, each techniques have their own pros and cons. While μ-XANES can demonstrated the spatial distribution of PFAS, it has limitation in detection limits and influence of inorganic fluoride. The CIC can differentiate the organofluoride and inorganic fluoride after the sample preparation steps to separate inorganic fluoride and organic fluoride in the ppb-range, though it is unable to visualize spatial distribution like μ-XANES and DESI. In turn, the ^{19}F NMR can directly analyse total organic fluoride. Camdzic et al. (2021) showed that ^{19}F NMR can clearly distinguish PFAS, non-PFAS, and F^- ions making samples preparation unnecessary. Although the ^{19}F NMR previously faced low sensitivity and was challenging to apply for solid matrix like concrete, it has been reported that its sensitivity for PFAS has been improved to 50 μg/L (Camdzic et al., 2023).

3.3. *Conclusions/future perspective*

The μ-XRF incorporated μ-XANES spectroscopy adds additional value in PFAS detection (i.e., inorganic fluorine, and ultrashort chain PFAS) to information gained from other techniques. On the other hand, μ-XANES can identify shorter chain PFAS and other fluorine compounds (e.g., TFMS and PFBS). μ-XRF mapping incorporated μ-XANES is a rapid and efficient method for PFAS group (ultrashort-, short-, and long-chain) detection. Our previous studies found that longer chain PFAS, especially PFOS, occur at their highest levels on the top part of the concrete sample ($P_1 - P_8$) (Thai et al., 2022; Vo et al., 2023). μ-XANES only found longer chain PFAS at the P_8 spot. This may be explained by the strong presence of inorganic fluorine (e.g., AlF_3, Na_2SiF_3), which might restrain the detectability of organic fluorine. This could be the reason for the low detection of PFAS on the top part of the concrete sample (Roesch et al., 2023). Using the LCF, we found that CaF_2, FeF_3, and Na_2SiF_3 might be the inorganic fluorine compounds in the concrete (Table S2). As described above, this is likely due to the standards that we used not being representative of the specific compounds for the LCF.

We acknowledge that this technique requires further work in testing additional concrete samples in either the same or different FTGs, and optimizing the peak ratio and LCF fitting to widespread its applicability. The limited access to beamline of μ-XANES spectroscopy also poses a challenge to popularize it to be a commercial analytical technique for PFAS in concrete.

The μ-XRF mapping incorporated μ-XANES spectroscopy has been used for the detection of PFAS in other matrices such as textile products, food packaging papers, baking sheets, sewage sludges, and soils (Roesch et al., 2023; Yan et al., 2021). The first benefit of using this hybrid technique is the ability to map out the heterogeneity of PFAS distribution in those samples. It visualizes the distribution of PFAS groups in the impacted concrete, even the distribution of PFAS coating on consumer products and fabric. The second benefit is the characterization of fluorine composition in one-sitting through μ-XANES, with PFAS inclusively. It provides a fast method for PFAS characterization in a matrix of interest (e.g., concrete). The method can be extended to other PFAS, but chemical standards and a suitable range of PFAS occurrence in the matrix, as well as the exact detection limits, must be considered in the future.

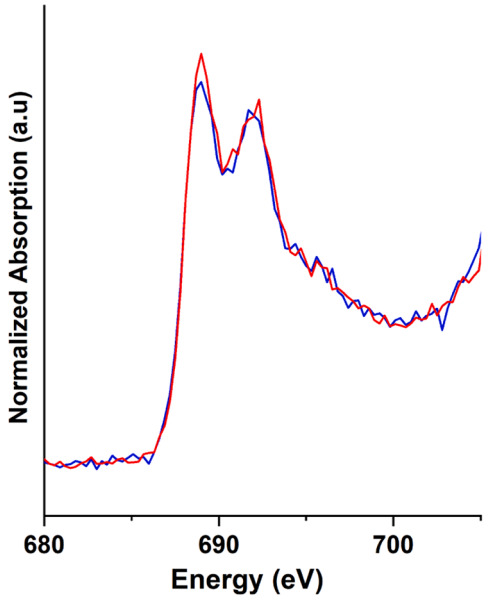

Fig. 2. Response of two fluorine K-edge μ-XANES scans at the same spot (blue color represents the first scan; red color represents the second scan) with a lateral resolution of 100 μm.

Funding informations

The Queensland Alliance for Environmental Health Sciences (QAEHS), The University of Queensland, gratefully acknowledges the financial support of Queensland Health. The study was supplemental to contract research for Arcadis and ExxonMobil Environmental and Property Solutions Company. Phong H. N. Vo is funded by University of Technology Sydney (UTS) Chancellor's Research Fellowship. J.F.M. is funded by an Australian Research Council (ARC) Laureate Fellowship. Furthermore, we acknowledge the Paul Scherrer Institute, Villigen, Switzerland, for the provision of synchrotron radiation beamtime at the PHOENIX beamline of the Swiss Light Source (SLS). We thank Camelia Borca and Thomas Huthwelker (SLS) for great beamline support. Lachlan Jekimovs (QAEHS) is acknowledged for providing comments and proof-reading.

CRediT authorship contribution statement

Phong Vo: Writing – original draft, Visualization, Methodology, Conceptualization. **Christian Vogel:** Writing – original draft, Visualization, Methodology, Investigation, Conceptualization. **Hong Nguyen:** Writing – review & editing, Validation. **Brett Hamilton:** Writing – review & editing, Validation. **Phong Thai:** Writing – review & editing, Conceptualization. **Philipp Roesch:** Writing – review & editing, Validation. **Franz-Georg Simon:** Writing – review & editing, Validation. **Jochen Mueller:** Writing – review & editing, Supervision, Conceptualization.

Declaration of Competing Interest

The authors declare the following financial interests/personal relationships which may be considered as potential competing interests: Jochen Mueller and Phong Thai reports financial support was provided by Queensland Health. Phong Vo reports financial support was provided by University of Technology Sydney. Jochen Mueller reports financial support was provided by Australian Research Council. If there are other authors, they declare that they have no known competing financial interests or personal relationships that could have appeared to influence the work reported in this paper.

Acknowledgment

The Queensland Alliance for Environmental Health Sciences (QAEHS), The University of Queensland, gratefully acknowledges the financial support of Queensland Health. The study was supplemental to contract research for Arcadis and ExxonMobil Environmental and Property Solutions Company. Phong H. N. Vo is funded by University of Technology Sydney (UTS) Chancellor's Research Fellowship. J.F.M. is funded by an Australian Research Council (ARC) Laureate Fellowship. Furthermore, we acknowledge the Paul Scherrer Institute, Villigen, Switzerland, for the provision of synchrotron radiation beamtime at the PHOENIX beamline of the Swiss Light Source (SLS). We thank Camelia Borca and Thomas Huthwelker (SLS) for great beamline support. Lachlan Jekimovs (QAEHS) is acknowledged for providing comments and proof-reading.

Appendix A. Supporting information

Supplementary data associated with this article can be found in the online version at doi:10.1016/j.hazl.2024.100134.

Data availability

Data will be made available on request.

References

Baduel, C., Paxman, C.J., Mueller, J.F., 2015. Perfluoroalkyl substances in a firefighting training ground (FTG), distribution and potential future release. J. Hazard. Mater. 296, 46–53. https://doi.org/10.1016/j.jhazmat.2015.03.007.

Camdzic, D., Dickman, R.A., Aga, D.S., 2021. Total and class-specific analysis of per- and polyfluoroalkyl substances in environmental samples using nuclear magnetic resonance spectroscopy. J. Hazard. Mater. Lett. 2, 100023. https://doi.org/10.1016/j.hazl.2021.100023.

Camdzic, D., Dickman, R.A., Joyce, A.S., Wallace, J.S., Ferguson, P.L., Aga, D.S., 2023. Quantitation of total PFAS including trifluoroacetic acid with fluorine nuclear magnetic resonance spectroscopy. Anal. Chem. 95 (13), 5484–5488. https://doi.org/10.1021/acs.analchem.2c05354.

van der Bom, F.J.T., Kopittke, P.M., Raymond, N.S., Sekine, R., Lombi, E., Mueller, C.W., Doolette, C.L., 2022. Methods for assessing laterally-resolved distribution, speciation and bioavailability of phosphorus in soils. Rev. Environ. Sci. Biotechnol. https://doi.org/10.1007/s11157-021-09602-z.

Douglas, G.B., Vanderzalm, J.L., Williams, M., Kirby, J.K., Kookana, R.S., Bastow, T.P., Bauer, M., Bowles, K.C., Skuse, D., Davis, G.B., 2023. PFAS contaminated asphalt and concrete - knowledge gaps for future research and management. Sci. Total Environ. 887, 164025. https://doi.org/10.1016/j.scitotenv.2023.164025.

Leeson, A., Thompson, T., Stroo, H.F., Anderson, R.H., Speicher, J., Mills, M.A., Willey, J., Coyle, C., Ghosh, R., Lebrón, C., Patton, C., 2021. Identifying and managing aqueous film-forming foam-derived per- and polyfluoroalkyl substances in the environment. Environ. Toxicol. Chem. 40 (1), 24–36. https://doi.org/10.1002/etc.4894.

Ravel, B., Newville, M., 2005. ATHENA, ARTEMIS, HEPHAESTUS: data analysis for X-ray absorption spectroscopy using IFEFFIT. J. Synchrotron Radiat. 12 (Pt 4), 537–541. https://doi.org/10.1107/s0909049505012719.

Roesch, P., Vogel, C., Huthwelker, T., Wittwer, P., Simon, F.-G., 2022. Investigation of per- and polyfluoroalkyl substances (PFAS) in soils and sewage sludges by fluorine K-edge XANES spectroscopy and combustion ion chromatography. Environ. Sci. Pollut. Res. 29 (18), 26889–26899. https://doi.org/10.1007/s11356-021-17838-z.

Roesch, P., Vogel, C., Wittwer, P., Huthwelker, T., Borca, C.N., Sommerfeld, T., Kluge, S., Piechotta, C., Kalbe, U., Simon, F.-G., 2023. Taking a look at the surface: μ-XRF mapping and fluorine K-edge μ-XANES spectroscopy of organofluorinated compounds in environmental samples and consumer products. Environ. Sci.: Process. Impacts 25 (7), 1213–1223. https://doi.org/10.1039/D3EM00107E.

Shelor, C.P., Warren, C., Odinaka, C.V., Dumre, K., 2024. Comprehensive review of combustion ion chromatography for the analysis of total, adsorbable, and extractable organic fluorine. J. Sep. Sci. 47 (15), 2400235. https://doi.org/10.1002/jssc.202400235.

Solé, V.A., Papillon, E., Cotte, M., Walter, P., Susini, J., 2007. A multiplatform code for the analysis of energy-dispersive X-ray fluorescence spectra. Spectrochim. Acta Part B: At. Spectrosc. 62 (1), 63–68. https://doi.org/10.1016/j.sab.2006.12.002.

Thai, P.K., McDonough, J.T., Key, T.A., Thompson, J., Prasad, P., Porman, S., Mueller, J.F., 2022. Release of perfluoroalkyl substances from AFFF-impacted concrete in a firefighting training ground (FTG) under repeated rainfall simulations. J. Hazard. Mater. Lett. 3, 100050. https://doi.org/10.1016/j.hazl.2022.100050.

Vo, P.H.N., Hamilton, B.R., Wepf, R.A., Key, T.A., Nguyen, T.M.H., Thai, P.K., Thomas, K., Mueller, J.F., 2023. Visualization of the distribution of PFOS and PFHxS in concrete by DESI MSI. Environ. Sci. Technol. Lett. 10 (5), 446–451. https://doi.org/10.1021/acs.estlett.3c00211.

Vogel, C., Rivard, C., Tanabe, I., Adam, C., 2016. Microspectroscopy – promising techniques to characterize phosphorus in soil. Commun. Soil Sci. Plant Anal. 47 (18), 2088–2102. https://doi.org/10.1080/00103624.2016.1228942.

Yan, B., Wang, J., Liu, J., 2021. STXM-XANES and computational investigations of adsorption of per- and polyfluoroalkyl substances on modified clay. Water Res. 201, 117371. https://doi.org/10.1016/j.watres.2021.117371.